

Hyaluronidase 3 (*HYAL3*) knockout mice do not display evidence of hyaluronan accumulation

Vasantha Atmuri^a, Dianna C. Martin^a, Richard Hemming^a, Alex Gutsol^{b,c}, Sharon Byers^{d,e}, Solmaz Sahebjam^f, James A. Thliveris^g, John S. Mort^f, Euridice Carmona^h, Judy E. Andersonⁱ, Shyamala Dakshinamurti^{b,c}, Barbara Triggs-Raine^{a,c,*}

^a Department of Biochemistry and Medical Genetics, The University of Manitoba, Winnipeg, MB, Canada

^b Department of Physiology, The University of Manitoba, Winnipeg, MB, Canada

^c Manitoba Institute for Child Health, Winnipeg, MB, Canada

^d Department of Paediatrics, and Genetics, The University of Adelaide, South Adelaide, Australia

^e Women's and Children's Hospital, South Adelaide, Australia

^f Shriners Hospital for Children, Montreal, QC, Canada

^g Department of Anatomy and Cell Science, The University of Manitoba, Winnipeg, MB, Canada

^h Maisonneuve-Rosemont Hospital, Research Centre and Department of Medicine, The University of Montreal, Montreal, QC, Canada

ⁱ Department of Biological Sciences, The University of Manitoba, Winnipeg, MB, Canada

ARTICLE INFO

Article history:

Received 21 April 2008

Received in revised form 18 July 2008

Accepted 29 July 2008

Keywords:

Hyaluronan

Hyaluronidase

Hyal3

Mucopolysaccharidoses

Glycosaminoglycan

ABSTRACT

Hyaluronidases are endoglycosidases that initiate the breakdown of hyaluronan (HA), an abundant component of the vertebrate extracellular matrix. In humans, six paralogous genes encoding hyaluronidase-like sequences have been identified on human chromosomes 3p21.3 (*HYAL2–HYAL1–HYAL3*) and 7q31.3 (*SPAM1–HYAL4–HYALP1*). Mutations in one of these genes, *HYAL1*, were reported in a patient with mucopolysaccharidosis (MPS) IX. Despite the broad distribution of HA, the *HYAL1*-deficient patient exhibited a mild phenotype, suggesting other hyaluronidase family members contribute to constitutive HA degradation. *Hyal3* knockout (*Hyal3*^{-/-}) mice were generated to determine if *HYAL3* had a role in constitutive HA degradation. *Hyal3*^{-/-} mice were viable, fertile, and exhibited no gross phenotypic changes. X-ray analysis, histological studies of joints, whole-body weights, organ weights and the serum HA levels of *Hyal3*^{-/-} mice were normal. No evidence of glycosaminoglycan accumulation, including vacuolization, was identified in the *Hyal3*^{-/-} tissues analyzed. Remarkably, the only difference identified in *Hyal3*^{-/-} mice was a subtle change in the alveolar structure and extracellular matrix thickness in lung-tissue sections at 12–14 months-of-age. We conclude that *HYAL3* does not play a major role in constitutive HA degradation.

Crown Copyright © 2008 Published by Elsevier B.V. All rights reserved.

1. Introduction

Hyaluronan (HA)¹ is a large unbranched glycosaminoglycan (GAG) comprised of repeating disaccharide units of *N*-acetyl D-glucosamine and D-glucuronic acid. It is an abundant component of the extracellular matrix of vertebrates, where it exists in both free and bound forms (Day and Prestwich, 2002). Although the ubiquitous distribution of HA has complicated investigations of its functions, clear roles for HA as a structural molecule and as a mediator of cellular signal transduction were demonstrated in mice deficient in HA synthase 2

(Camenisch et al., 2000). Given the rapid turnover rate of HA, with approximately one-third or 5 g of the human body's HA turned over each day (Laurent and Reed, 1991), and the critical functions of HA, hyaluronidase enzymes that initiate HA degradation are presumed to be essential (Rodan et al., 1989).

Hyaluronidase was initially observed by Duran-Reynals as a “spreading factor” that facilitates the diffusion of subcutaneously injected vaccines, dyes and toxins (Kreil, 1995). Through analyses of human genome sequences, hyaluronidases have been identified as members of a multigene family comprised of six paralogs, five of which predict protein products with approximately 40% identity. These sequences are localized as two clusters, on human chromosomes 3p21.3 (*HYAL2–HYAL1–HYAL3*) and 7q31.3 (*SPAM1–HYAL4–HYALP1*) (Csoka et al., 1999; Csoka et al., 2001). The equivalent clusters are found on mouse chromosomes 9F1–F2 and 6A2, respectively (Csoka et al., 2001). In addition, the mouse has a seventh paralog, *Hyal5*, on chromosome 6A2, downstream of *HyalP1* (Kim et al., 2005). Except for *HYALP1*, which is a pseudogene in humans, these

* Corresponding author. Department of Biochemistry and Medical Genetics, The University of Manitoba, 770 Bannatyne Ave., Winnipeg, MB, Canada R3E 0W3. Tel.: +1 204 789 3218; fax: +1 204 789 3900.

E-mail address: traine@ms.umanitoba.ca (B. Triggs-Raine).

¹ Abbreviations: HA – hyaluronan; GAG – glycosaminoglycan; MPS – mucopolysaccharidosis; GPI – glycosylphosphatidylinositol; neo – neomycin resistance cassette; ES – embryonic stem; RT – reverse transcription; PGK – phosphoglycerate kinase; β-Hex – β-hexosaminidase; TK – thymidine kinase.

genes have protein products that are known or suggested to be involved in HA and/or chondroitin sulfate degradation (Stern and Jedrzejak, 2006).

In a rat model, intravenously injected HA is found to be degraded locally (10–30%) or is cleared from the tissues and degraded through the lymph nodes (50–90%). The remaining HA enters the blood stream where it is removed by the liver, kidney and spleen (Fraser and Laurent, 1989). HA receptors that are required for the uptake of HA prior to degradation have been identified in these various tissues. The degradation of HA is primarily believed to take place in the lysosome, since the addition of ammonium chloride, a weak base that disrupts lysosomal function, prevents HA degradation (Culty et al., 1992). This lysosomal HA degradation is presumably initiated through the endoglycolytic action of hyaluronidases and sustained through the action of the lysosomal exoglycosidases, β -glucuronidase and β -hexosaminidase (β -Hex) which are able to cleave the individual sugar residues of HA from the non-reducing terminus (Rodan et al., 1989).

Evidence suggesting hyaluronidases contribute to HA degradation was strengthened with the diagnosis of a patient with mucopolysaccharidosis (MPS) IX (Natowicz et al., 1996). The absence of detectable *HYAL1* activity due to mutations in its gene (Triggs-Raine et al., 1999) resulted in a 38 to 90 fold increase in serum HA and lysosomes in skin fibroblasts and macrophages from the MPS IX patient were filled with HA. Compared to patients with other MPS disorders, this patient displayed mild clinical features including soft masses near various joints, mild short stature, erosions of the hip joint, a flattened nasal bridge and submucosal cleft palate. The mild phenotype of this MPS IX patient despite the broad distribution of HA, and the identification of multiple hyaluronidases, suggested that other hyaluronidases play a major role in HA degradation. Among the family of hyaluronidases, only *HYAL1*, *HYAL2* and *HYAL3* are broadly expressed (Csoka et al., 1999). The identification of *HYAL2* as a glycosylphosphatidylinositol (GPI)-linked protein that is found in the plasma membrane of some cells (Rai et al., 2001) made *HYAL3* a good candidate to play a role in HA degradation based on its intracellular localization. We generated a mouse model with a deficiency of *HYAL3* in order to evaluate its role in HA degradation. Herein we have characterized the basic macroscopic and microscopic characteristics of this model, focusing on the tissues with high *Hyal3* expression (Csoka et al., 1999) and/or high HA turnover (Fraser et al., 1997) for evidence of HA accumulation. These *Hyal3*^{-/-} animals were apparently normal and no GAG accumulation was detectable, suggesting that under normal circumstances, *HYAL3* does not contribute significantly to HA degradation.

2. Results

2.1. Generation of *Hyal3* knockout mice

The targeting vector shown in Fig. 1A was used to disrupt *Hyal3* by introducing a neomycin resistance cassette (neo) into exon 2 of the *Hyal3* gene at the NsiI site. This targeting construct was designed to disrupt *Hyal3* while having minimal impact on an overlapping gene, *Fus2* (*N*-acetyltransferase 6) (Shuttleworth et al., 2002). The second exon of *Fus2* is imbedded within the first intron of *Hyal3* (Fig. 1A). By inserting “neo” in exon 2 of *Hyal3*, downstream from the last exon of *Fus2*, we expected normal transcription of both *Fus2* and *Hyal3*, but that the *Hyal3* transcripts would be abnormal and would not encode functional protein.

To identify embryonic stem (ES) cell clones that had neo correctly inserted into *Hyal3*, we screened 98 G418-resistant and gangcyclovir sensitive ES cell clones by Southern analysis. Seven correctly targeted ES cell clones were identified by the presence of a 12.9 kb NdeI fragment (wild-type fragment is 10.9 kb) using a 5' external probe (probe “a” in Fig. 1A). Hybridization results for the two correctly

targeted ES cell clones (below) are shown in Fig. 1B. The correct homologous recombination event was confirmed by Southern analysis of NdeI-digested DNA using a 3' external probe (probe “c” in Fig. 1A), and the presence of only one neo insertion was confirmed using a neo-specific probe (probe “b” in Fig. 1A) (data not shown). As well, Southern analysis of NsiI-digested DNA with all three probes reconfirmed that correct targeting had taken place (data not shown).

Chimeras with germ-line transmission of the targeted *Hyal3* allele were obtained for each of the two independently targeted ES cell lines by aggregation with *CD1* embryos. These chimeras were crossed with *CD1* female mice to generate two independent *CD1*;*129S1* lines. One of the two chimeras was also crossed with *129S1* female mice to generate a congenic *129S1* line. The genotypes of offspring were initially defined by Southern analysis of DNA isolated from liver tissue. The targeted *Hyal3* allele in *Hyal3*^{+/-} and *Hyal3*^{-/-} mice was identified as a 12.9 kb NdeI band (Fig. 1B). Southern analysis was replaced by PCR amplification of tail-clip DNA for routine genotyping. The *Hyal3* targeted and wild-type alleles were identified as 1.0 kb and 0.5 kb bands respectively (Fig. 2C). Genotypes were identified by the presence of only the 0.5 kb wild-type band (+/+), only the 1.0 kb neo-targeted band (-/-) or both the 0.5 and 1.0 kb bands (+/-).

2.2. Analysis of the expression of *Hyal3* and *Fus2* from the targeted locus

To determine how the *Hyal3*-targeting event affected the expression of *Hyal3* and *Fus2*, transcript levels of *Hyal3* and *Fus2* were examined by real-time reverse transcription (RT)-PCR using total RNA isolated from testis and liver of 8 to 12 month-old *Hyal3*^{-/-} and *Hyal3*^{+/+} mice as templates. Testis was chosen because this tissue has a high level of both *Hyal3* and *Fus2* expression; liver was chosen as the non-

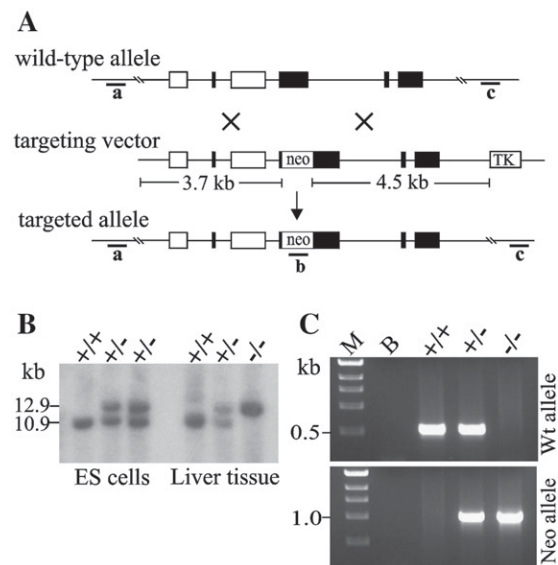


Fig. 1. Targeted disruption of the *Hyal3* gene. (A) The *Hyal3* screening strategy. *Hyal3* wild-type allele, targeting vector and targeted allele are represented as consecutive lines. Large solid boxes and lines, respectively, represent the exons and introns of *Hyal3*; large open boxes represent the exons of *Fus2*. Small solid boxes (labelled as “a”, “b” or “c”) below the lines represent probes used for Southern hybridization. The regions of homology are indicated as 3.7 and 4.5 kb. Inserted neomycin (neo) and thymidine kinase (TK) cassettes used as positive and negative selection markers are depicted as labeled open boxes. “/” represents a break in the sequence. This figure is not drawn to scale. (B) Southern analysis of *Hyal3*. Genomic DNA isolated from ES cell clones or mouse liver was digested with NdeI and screened for “neo” insertion using the 5' external probe (“a”). The targeted allele was detected as a 12.9 kb band, and the wild-type allele as a 10.9 kb band. ES cell clones or mouse liver tissues were identified as +/+ (only 10.9 kb band), -/- (only 12.9 kb band) and +/- (both 10.9 and 12.9 kb bands). (C) PCR amplification of genomic DNA. The genotypes of *Hyal3* mice were identified by amplification of tail-clip genomic DNA with primers specific for the wild-type allele (top panel) or the targeted (neo) allele (bottom panel). M—molecular-weight marker; B—No template control.

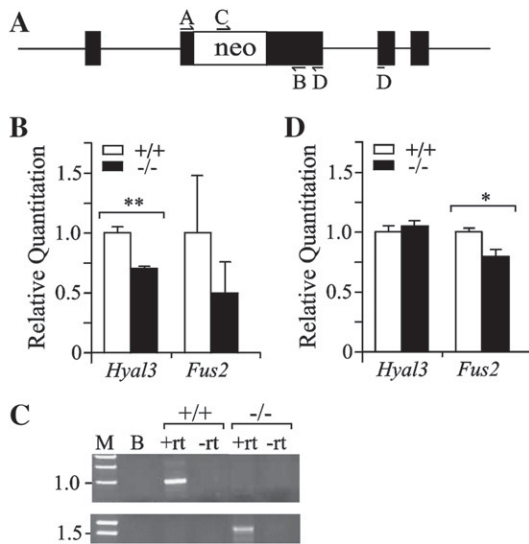


Fig. 2. Characterization of *Hyal3* and *Fus2* transcripts. (A) Schematic of the positions of PCR primers used to characterize the neo-targeted *Hyal3* allele by conventional RT-PCR. Exons are shown as solid boxes, introns as straight lines and the neo insertion as an open box. The positions of primers are shown as arrows and labeled as “A”, “B”, “C” and “D”. (B) Expression levels of *Hyal3* and *Fus2* in the testis of *Hyal3*^{-/-} and *Hyal3*^{+/+} mice by real-time RT-PCR. The mean (\pm SD) ΔC_T values of *Hyal3* and *Fus2* transcripts in *Hyal3*^{-/-} mice are represented as a proportion of the mean (\pm SD) ΔC_T values of *Hyal3* and *Fus2* transcripts in *Hyal3*^{+/+} mice ($n=3$; ** $P=0.001$ [*Hyal3*], $P=0.22$ [*Fus2*]). (C) Characterization of *Hyal3* transcripts by conventional RT-PCR. Total RNA isolated from the testis of *Hyal3*^{-/-} and *Hyal3*^{+/+} mice was reverse-transcribed and PCR-amplified using primer sets (A) specific for the wild-type (top panel) and the targeted allele (bottom panel). M—1 kb DNA ladder, B—control without cDNA, -rt—cDNA without reverse transcriptase and +rt—cDNA with reverse transcriptase. (D) Expression levels of *Hyal3* and *Fus2* in the liver of *Hyal3*^{-/-} and *Hyal3*^{+/+} mice by real-time RT-PCR. The mean (\pm SD) ΔC_T values of *Hyal3* and *Fus2* transcripts in *Hyal3*^{-/-} mice are represented as a proportion of the mean (\pm SD) ΔC_T values of *Hyal3* and *Fus2* transcripts in *Hyal3*^{+/+} mice ($n=3$, $P=0.23$ [*Hyal3*], * $P=0.03$ [*Fus2*]).

reproductive tissue with the highest expression of both *Hyal3* and *Fus2* (Shuttleworth et al., 2002).

Real-time RT-PCR studies using primers that span the boundary between exon 2 and exon 3 of *Hyal3* (TaqMan assay; Mm00662097_m1) demonstrated the presence of *Hyal3* transcripts in both *Hyal3*^{-/-} and *Hyal3*^{+/+} mice. The level of *Hyal3* transcripts was reduced by approximately one-third in the testis of *Hyal3*^{-/-} mice compared to *Hyal3*^{+/+} controls (Fig. 2B, $n=3$, $P=0.001$), although the levels of *Hyal3* transcripts detected in the liver of *Hyal3*^{-/-} and *Hyal3*^{+/+} mice were not different (Fig. 2D, $n=4$, $P=0.23$). The presence of *Hyal3* mRNA in *Hyal3*^{-/-} mice was expected, but in order to confirm that these were aberrant *Hyal3* transcripts, they were characterized by conventional RT-PCR. Using sense and antisense primers flanking the *neo* insertion site, and within exon 2 (primers A and B in Fig. 2A), PCR products (920 bp) were generated only from the cDNA of *Hyal3*^{+/+} mice (Fig. 2C, top panel). PCR products were not generated from the cDNA of the *Hyal3*^{-/-} mice under any of the conditions that were tested, indicating that normal *Hyal3* transcripts are absent in the *Hyal3*^{-/-} mice. To confirm that the *Hyal3* transcripts produced in the *Hyal3*^{-/-} mice contained some part of *neo*, the cDNA was amplified with a sense primer (Primer “C” in Fig. 2A) within *neo* and an antisense primer (Primer “D” in Fig. 2A) that spanned the junction of *Hyal3* exons 2 and 3. Amplification using these primers was only detected in the cDNA generated from *Hyal3*^{-/-} testis and not *Hyal3*^{+/+} testis (Fig. 2C, bottom panel).

Real-time RT-PCR using primers within exon 2 of *Fus2* (TaqMan assay; Mm01947825_S1) demonstrated that *Fus2* transcripts were not significantly altered in *Hyal3*^{-/-} mouse testis (Fig. 2B, $n=3$, $P=0.22$). However, the levels of *Fus2* transcripts were reduced by approximately 20% in the liver of *Hyal3*^{-/-} mice compared to *Hyal3*^{+/+} mice (Fig. 2D, $n=4$, $P=0.03$).

Taken together, the real-time and conventional RT-PCR data showed that the testis and liver of *Hyal3*^{-/-} mice contained no

detectable normal *Hyal3* transcripts, but did have *Hyal3* transcripts containing the *neo* insertion. It is likely that the *Hyal3* transcripts detected in *Hyal3*^{-/-} mice originate in the neomycin resistance gene, under the control of the phosphoglycerate kinase (PGK) promoter. These transcripts would not have exon 1 or the beginning of exon 2 of *Hyal3*, since this is where the *neo* cassette is inserted. The abnormal transcripts would not direct the synthesis of any normal *HYAL3* protein. Unfortunately, *HYAL3* protein levels in normal mice were not sufficient to convincingly assay the protein. Therefore, the absence of *HYAL3* could not be confirmed in *Hyal3*^{-/-} mouse tissues (data not shown).

2.3. Macroscopic phenotype of *Hyal3* knockout mice

Hyal3^{-/-} mice of both *CD1;129S1* (mixed) and *129S1* (congenic) background appeared healthy and normal in appearance up to 18 months-of-age, the latest time point examined. Both males and females were fertile and litter sizes appeared normal. Combined data from crosses between *Hyal3* heterozygotes (+/-) of both mixed and congenic background resulted in offspring with a normal Mendelian ratio of wild-type (+/+), heterozygous (+/-) and homozygous (-/-) mice ($\chi^2=0.45$, $P=0.80$, $n=146$). There was no difference from the expected 1-to-1 ratio of affected male to female offspring ($\chi^2=1.34$, $P=0.25$, $n=146$). X-ray analysis of the skeleton of 12 to 14 month-old *Hyal3*^{-/-} and *Hyal3*^{+/+} mice ($n=5$), and visual examination of joints did not reveal any obvious abnormalities. There was also no difference between total body weight of *Hyal3*^{-/-} and *Hyal3*^{+/+} mice at either 6 or 12 months-of-age (Fig. 3A). At necropsy, organ morphology and size appeared normal, and there was no difference in organ weights at 12 (Fig. 3B), 6 or 14 months-of-age (data not shown). Thus, *Hyal3*^{-/-} mice have no obvious gross phenotype and lack the skeletal features that were identified in the MPS IX patient.

2.4. Analysis of serum HA levels

Serum HA concentration was determined because the elevated serum HA level (38 to 90 fold normal) in the MPS IX patient suggested

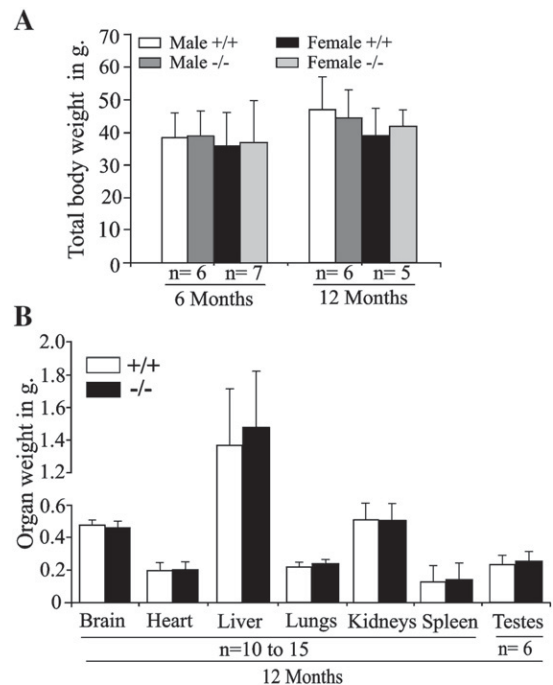


Fig. 3. Body and organ weight of *Hyal3*^{-/-} mice. (A) The mean (\pm SD) body weight (g) of male and female mice at 6 to 12 months-of-age ($P>0.05$). (B) Mean (\pm SD) organ weights of 12 month-old mice ($P>0.05$).

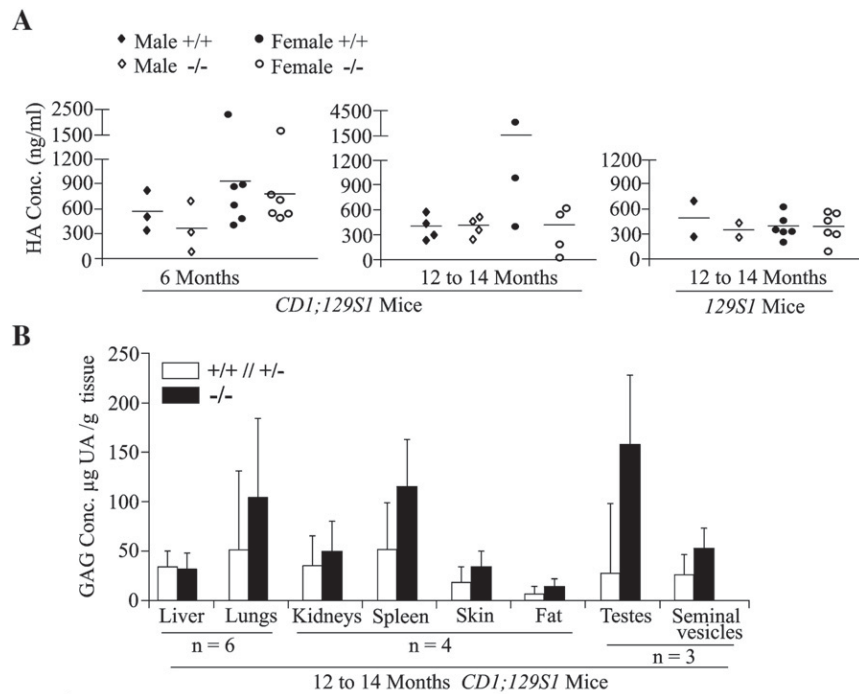


Fig. 4. Biochemical analyses of serum HA and tissue GAGs. (A) Serum HA analysis. Serum HA concentration from both mixed and congenic lines of *Hyal3*^{-/-} and *Hyal3*^{+/+} mice is shown. Each point represents the value of an individual animal and the horizontal line represents the mean value. (B) Total GAG concentration. Total tissue-GAG content was determined by uronic acid assay and is represented as the mean GAG concentration in tissues of 12–14 month-old male and female mice (*CD1;129S1*, n=3 to 6). The mean±SD are plotted for each tissue ($P>0.05$).

it could be an indicator of HA accumulation. Therefore, serum HA was measured in *Hyal3*^{-/-} and *Hyal3*^{+/+} mice of both mixed and congenic background using an ELISA assay. No elevation in serum HA was identified in *Hyal3*^{-/-} mice of either line at any age examined (Fig. 4A). Serum HA levels of the mixed line exhibited large variations making these results difficult to compare. However, no statistically significant elevation in HA ($P>0.05$) was identified in *Hyal3*^{-/-} mice compared to *Hyal3*^{+/+} mice matched for age, strain and gender even in the congenic

129S1 mice that exhibited less individual variation. These results indicate that *Hyal3*^{-/-} mice lack the serum HA elevation characteristic of the MPS IX patient.

2.5. Analysis of tissue GAG levels

Tissue GAG content was examined to determine whether any tissues from the *Hyal3*^{-/-} mice exhibited GAG accumulation. Total

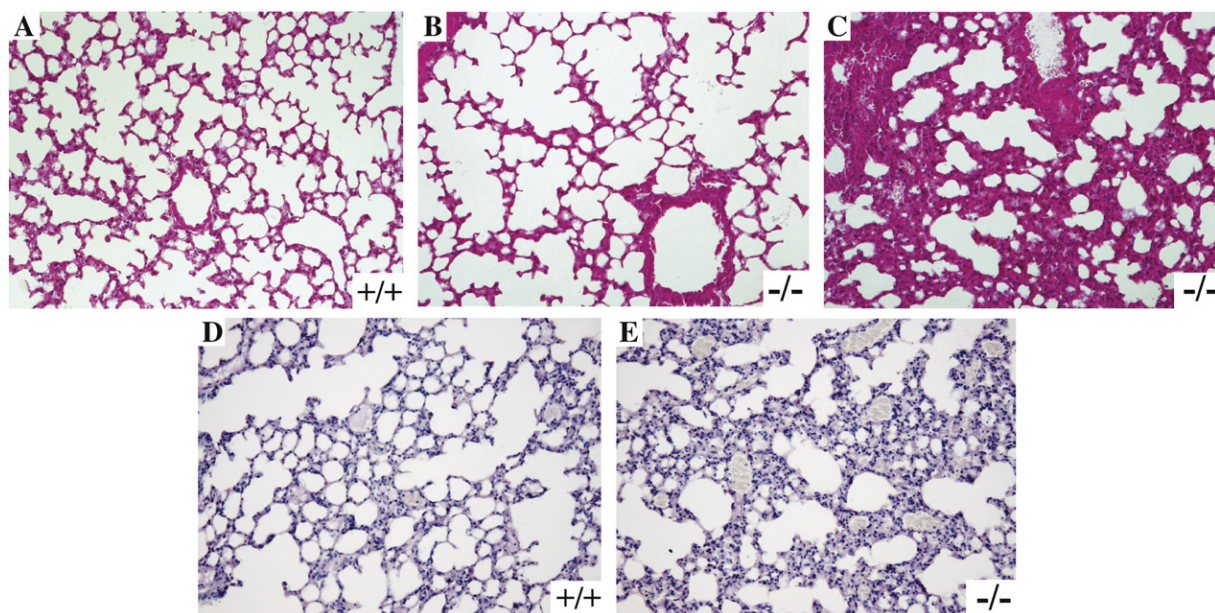


Fig. 5. Histology of lung tissue in *Hyal3*^{-/-} and *Hyal3*^{+/+} mice. Lung tissues from 12–14 month-old *Hyal3*^{-/-} mice (n=6, *129S1*) exhibited larger alveoli (B) and more areas of thickened extracellular matrix (C) compared to wild-type mice lungs (A). Lung tissues from 6 month-old *Hyal3*^{-/-} mice (n=2, *CD1;129S1*) showed more immature alveoli (E) compared to *Hyal3*^{+/+} mice (D).

GAGs were determined in tissues with high rates of HA turnover (liver, kidney, spleen and skin) and *Hyal3* expression (testis) (Shuttleworth et al., 2002), as well as lung, fat and seminal vesicle. GAG content was estimated using an assay for uronic acid that would detect both HA and chondroitin sulfate, the two substrates of hyaluronidase (Stern and Jedrzejewski, 2006). There was no difference between the GAG content of tissues from 12–14 month-old *Hyal3*^{-/-} and control mice (*CD1;129S1*) (Fig. 4B).

2.6. Histological studies

A broad range of tissues, including liver, skin, lung, brain, fat, testis, seminal vesicle, ovary, uterus, kidney, heart, muscle, eye and lymph node were used to examine general morphology, with particular scrutiny for extracellular or intracellular HA accumulation (vacuolization). No consistent difference in tissue organization or connective tissue thickness was identified between tissues of the *Hyal3*^{-/-} and *Hyal3*^{+/+} mice except in the lung (see below). Subsets of the tissues with either high rates of HA turnover (lymph node, skin and liver) or high levels of *Hyal3* expression (testis and brain), together with lung tissue were also examined by electron microscopy. There was no evidence of cellular vacuolation in *Hyal3*^{-/-} tissues, even in the tissues from 12–14 month-old *Hyal3*^{-/-} mice, where HA accumulation would be expected to be greatest (*n*=2). Moreover, we didn't detect any abnormality in lung interstitial regions by electron microscopy (*n*=4).

The skeletal system is often affected in mucopolysaccharidoses because of the abundance of GAGs in skeletal tissues. Indeed, the MPS IX patient displayed acetabular erosion and nearby fluid-filled masses. The role of *Hyal3* in joints was assessed by examining sections of knee-joint-tissues from *Hyal3*^{-/-} mice at 12–14 months-of-age (*CD1;129S1*, *n*=3). Sections were stained with toluidine blue which detects tissue proteoglycans. Joint-tissue sections were also stained for proteoglycans with Safranin O (*n*=1) or for HA by immunostaining for HA-binding protein (*n*=1). Overall, no difference was observed between the knee-joint-tissues from the *Hyal3*^{-/-} and *Hyal3*^{+/+} mice, indicating that *HYAL3* does not have a major role in GAG degradation in the joints.

In *Hyal3*^{-/-} mice, out of all the tissues analyzed, only lung-tissue histology was abnormal. Lung tissue from 12–14 month-old *Hyal3*^{-/-} mice (*129S1*, *n*=6) had abnormally large alveolar sacs (Fig. 5B) compared to *Hyal3*^{+/+} mice (Fig. 5A). A thickened interstitium was also found in a larger proportion of the lungs from *Hyal3*^{-/-} mice compared to controls (Fig. 5C). Preliminary studies of lung tissues from *Hyal3*^{-/-} mice at 6 months-of-age showed more immature alveoli (Fig. 5E, *n*=2, *CD1;129S1*) compared to the age-matched controls (Fig. 5D). However, quantitative studies were not possible as the lungs were not inflated for fixation. Further studies to confirm and extend these findings are in progress.

2.7. Expression of other genes involved in HA breakdown

HA accumulation was not detected in any of the examined tissues or serum from *Hyal3*^{-/-} mice, despite the absence of normal *Hyal3* transcripts. To determine if a *HYAL3* deficiency was compensated by other genes involved in HA breakdown, we analyzed the expression of two broadly expressed hyaluronidases (*Hyal1* and *Hyal2*) by real-time RT-PCR. The expression of these genes was analyzed in testis and liver tissues from 8–12 month-old *Hyal3*^{-/-} and *Hyal3*^{+/+} mice (*CD1;129S1*). There was no difference in the expression of *Hyal1* or *Hyal2* in the testis (Fig. 6A, *n*=3) (*Hyal1*, *P*=0.08; *Hyal2*, *P*=0.42) of *Hyal3*^{+/+} and *Hyal3*^{-/-} mice. In liver tissue, however, the expression of *Hyal1* was reduced by 60% (Fig. 6B, *n*=4, *P*=0.02) although *Hyal2* did not change significantly (Fig. 6B, *n*=4, *P*=0.09). The expression of other hyaluronidases in testis, *Hyal4*, *Hyal5*, *Hyalp1* and *Spam1* was also not different between *Hyal3*^{-/-} and *Hyal3*^{+/+} mice (Fig. 6A, *n*=3).

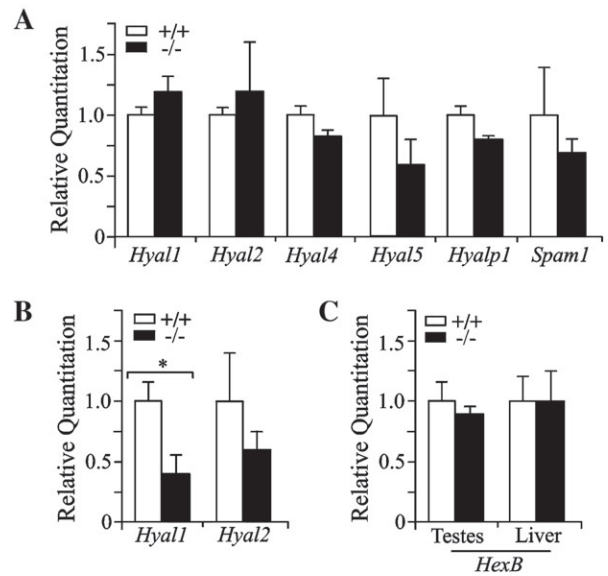


Fig. 6. Expression levels of possible compensating enzymes by real-time RT-PCR. The mean (\pm SD) $\Delta\Delta C_T$ values of the transcripts of the individual genes in *Hyal3*^{-/-} mice are represented as a proportion of their mean (\pm SD) $\Delta\Delta C_T$ values in *Hyal3*^{+/+} mice. (A) Expression levels of hyaluronidases in the testis (*CD1;129S1*, *n*=3; *P*=0.08 [*Hyal1*], *P*=0.42 [*Hyal2*], *P*=0.13 [*Hyal4*], *P*=0.12 [*Hyal5*], *P*=0.06 [*Hyalp1*], *P*=0.23 [*Spam1*]). (B) Expression levels of *Hyal1* and *Hyal2* in the liver, (*n*=4; *P*=0.02 [*Hyal1*]; *P*=0.09 [*Hyal2*]), (C) Expression levels of *HexB* in the testis (*n*=3, *P*=0.5) and liver (*n*=4, *P*=0.90).

The exoglycosidases, β -Hex and β -glucuronidase are the enzymes that release terminal sugar moieties from the HA-breakdown products of hyaluronidases, and could also compensate for a hyaluronidase deficiency. The expression of one of these exoglycosidases, *HexB*, was analyzed in the testis and liver tissues of *Hyal3*^{-/-} and *Hyal3*^{+/+} mice by real-time RT-PCR. No difference in *HexB* expression was observed in either the testis (Fig. 6C, *n*=3, *P*=0.50) or liver (Fig. 6C, *n*=4, *P*=0.90). Furthermore, β -Hex activity was also analyzed using an enzymatic assay. Again, β -Hex activity in liver of 12–14 month-old *Hyal3*^{-/-} and *Hyal3*^{+/+} mice was unchanged (*CD1;129S1*, *n*=8, *P*=0.14, data not shown). Overall, the absence of hyaluronidase or exoglycosidase elevation suggested that these enzymes are not compensating for *Hyal3* deficiency.

3. Discussion

The mild phenotype found in a *HYAL1*-deficient patient, despite the broad distribution and rapid turnover of HA, suggests that other hyaluronidases play an important role in HA degradation. Among the other hyaluronidases, we considered *HYAL3* as the most likely hyaluronidase to participate in HA degradation because of its broad expression (Shuttleworth et al., 2002) and intracellular localization (Hemming et al., 2008). *HYAL2* is also broadly expressed, but its localization is controversial (Chow et al., 2006; Miller, 2003). *HYAL2* also appears to be active only toward high molecular-weight HA (Lepperdinger et al., 1998), making it unlikely to play a major role in intracellular HA breakdown. We have now generated and characterized a *Hyal3* deficient mouse model. Based on comprehensive studies of our model, *HYAL3* does not have a major role in the constitutive degradation of HA.

Our studies employed a *Hyal3*-targeting vector that was designed to disrupt *Hyal3* function while maintaining normal transcription of an overlapping gene, *Fus2*. In *Hyal3*^{-/-} mice, transcripts were produced from *Hyal3*, but they were abnormal and did not include the full exon 2 coding sequence. The abnormal transcript would not encode a functional *HYAL3* protein as exon 2 is highly conserved among all of the hyaluronidases and site-directed mutagenesis studies have

demonstrated that the key active-site residues are within this region (Arming et al., 1997). Furthermore, changes as small as single amino acid substitutions lead to misfolding of glycoproteins. If any parts of *HYAL3* protein are translated from the abnormal transcripts, they would not have a signal sequence, would not be glycosylated, and thereby could not fold to form a functional protein.

Real-time RT-PCR demonstrated that the transcription of the overlapping gene, *Fus2*, was preserved in the testis of the new model of *Hyal3*^{-/-} mice used for this study (Fig. 2B), although *Fus2* transcripts in the liver were reduced by 20% of the level in wild-type mouse liver (Fig. 2D). Therefore the targeting construct was successful in disrupting *Hyal3* while maintaining substantial levels of *Fus2* expression. Interestingly, the level of *Hyal1* expression was also slightly reduced in the liver (Fig. 6B). There are many co-transcripts in the liver that include *Hyal1* and/or *Fus2* and/or *Hyal3* (Shuttleworth et al., 2002). The disruption of normal *Hyal3* transcription may interfere with the expression of these co-transcripts and therefore both *Hyal1* and *Fus2* transcripts would be lowered. This interference could be direct due to the destabilization of the transcripts or it may be the indirect results of *Hyal3* deficiency. In previous work, our laboratory showed that overexpression of *Hyal3* increased *Hyal1* expression (Hemming et al., 2008), suggesting that a feedback loop exists; therefore a decrease in *Hyal3* transcripts could decrease *Hyal1* and *Fus2* transcripts. *Fus2* encodes a cytoplasmic *N*-acetyltransferase, and has been localized in a region associated with lung-cancer susceptibility (Zegerman et al., 2000). Given this, changes in *Fus2* expression must be considered as a possible confounding variable in the interpretation of the lung phenotype in the *Hyal3*^{-/-} mice.

HA is broadly distributed, and the highest concentrations are found in connective tissues. Accordingly, while evidence of HA accumulation was investigated in a broad range of tissues, the present survey placed the greatest emphasis on the tissues where high turnover of HA is expected or *Hyal3* expression is high. Neither biochemical nor histological approaches detected any evidence of GAG accumulation. These results indicate that *HYAL3* is not a major contributing enzyme to the constitutive degradation of any GAG, including HA.

The skeletal system is most affected in the *HYAL1*-deficient human (Natowicz et al., 1996) and was the only system where HA accumulation was detected in *Hyal1*^{-/-} mice (Martin et al., 2008). Considering the high HA turnover in joint tissue, we specifically examined the knee joint in *Hyal3*^{-/-} mice, but there was no evidence of HA accumulation. This finding indicates that *HYAL3* does not have a major role in the constitutive degradation of HA, even in high-turnover tissues.

Despite the lack of HA accumulation in skeletal and non-skeletal tissues of *Hyal3*^{-/-} mice, the lung-tissue morphology was abnormal. Lung tissue from aged *Hyal3*^{-/-} mice displayed large alveoli and a larger proportion of lung area had a thickened interstitium compared to lung tissue from age-matched wild-type mice. In preliminary studies of young *Hyal3*^{-/-} mice, fewer septa were identified in alveoli, suggesting *HYAL3* deficiency may lead to age-dependent development of an alveolar-septal defect. Unfortunately, quantitative studies were not possible as the lungs were not inflated to a set pressure prior to fixation. Detailed analysis of lung histology and *Fus2* expression in this tissue is necessary to confirm that these findings are due to *HYAL3* deficiency. It is interesting to note, however, that *HYAL1*, *HYAL2*, and *HYAL3* all exhibit relatively high expression in the lung, consistent with the important role of HA in maintaining normal lung function (Jiang et al., 2005).

The absence of GAG accumulation in *Hyal3*^{-/-} mouse tissues was not surprising since recent work from our lab using *HYAL3* over-expressing cells (Hemming et al., 2008) and the work of others (Harada and Takahashi, 2007) indicated that *HYAL3* lacks hyaluronidase activity. Of note, although *HYAL3* did not have intrinsic enzymatic activity, *HYAL1* activity was increased in *HYAL3* over-expressing cells (Hemming et al., 2008). This putative non-enzymatic role for *HYAL3* in

HA metabolism is supported by other recent work from our laboratory on *HYAL1*-deficient mice, which had an approximate 5-fold increase in *Hyal3* mRNA (Martin et al., 2008). This reciprocal interplay between *HYAL1* activity and *Hyal3* expression indicates a cooperative role for *HYAL1* and *HYAL3* in HA metabolism. It is also possible that *HYAL3*'s function depends on the presence of a co-factor that is only present in specific cell types and would not have been present in the cell lines used for *in vitro* expression analysis. Given that 60% of the monocytes/macrophages in the body are found in the lung tissue, it is possible that monocytes contain such a co-factor, and therefore a deficiency of *HYAL3* would be most evident in the lungs.

We analyzed the transcripts of other enzymes that might contribute to HA degradation in *Hyal3*^{-/-} mice tissues since these enzymes might be upregulated to compensate for *HYAL3* deficiency in the testis tissue where *Hyal3* expression is normally highest. No increase in the expression of any of the hyaluronidases or the exoglycosidase, β -Hex, was identified. This may not be extremely surprising given the very low expression level of *Hyal3* compared to the other hyaluronidases. *HYAL2* may still be a reasonable candidate to compensate for loss of *HYAL1* activity, especially when combined with the very abundant lysosomal exoglycosidases, β -glucuronidase, and β -Hex. Although *HYAL2* has a GPI-linked cell surface form, some enzyme is found in early endosomes, suggesting that it could play a role in both extracellular and intracellular HA catabolism.

Present studies of *Hyal3*^{-/-} mice indicate that *HYAL3* is not a major contributor to constitutive HA degradation. Together with other studies, these findings suggest that *HYAL3* is not a classic hyaluronidase but instead has another role in HA metabolism. However, it is clear from this study, and that of *HYAL1*-deficient mice (Martin et al., 2008) that there is still much to be understood about the mechanism of HA degradation. Studies of double knockouts of *Hyal1* and *Hyal3* will be essential to unravel some of the unanswered questions in HA catabolism and MPS pathophysiology.

4. Experimental procedures

4.1. Construction of the *Hyal3*-targeting vector

The mouse *Hyal1*, *Hyal2* and *Hyal3* genes were mapped on a mouse genomic 129/Sv PAC clone, 452D10, as part of a previous study (Shuttleworth et al., 2002). A 10.8 kb *S*all subclone containing *Hyal1*, pHLS1, and an 8.75 Kb *S*all/*P*meI subclone containing *Hyal3*, pHLS3, were used as sources for the homologous arms of the targeting vector. A neo cassette from pGT-N28 (New England Biolabs, Beverly, MA, USA) containing the neomycin resistance gene under the control of the PGK promoter was introduced into the *N*siI site of exon 2 of *Hyal3* (Fig. 1A), 40 bp downstream of its initiation codon. The herpes simplex virus type 1 thymidine kinase (TK) gene under the control of the PGK promoter was isolated from pGEM7TK (Adra et al., 1987) and introduced at the 3' end of the 4.5 kb homologous arm of the targeting vector. The 5' homologous arm was extended to 3.7 kb by introducing an additional 2.7 kb *S*al1/*E*coRI fragment from pHLS1 into the *S*all site upstream of *Hyal3*. The final targeting construct contained 3.7 kb and 4.5 kb of 5' and 3' homology, respectively (Fig. 1A).

4.2. Selection and identification of targeted ES cells

The *Hyal3*-targeting vector was linearized with *Not*I restriction enzyme and introduced into R1 embryonic stem ES cells derived from 129/SvEv mice using electroporation. The electroporation and the selection of targeted cells on G418 and gangcyclovir were performed as described previously (Nagy et al., 2003). On days 9 and 10 post-electroporation, 168 G418-resistant ES cell colonies were picked and grown for screening and potential storage. DNA was prepared as described (Nagy et al., 2003), digested with *Nde*I and screened by

Southern hybridization with probe “a” (Fig. 1A) which spans nucleotides 6488498 to 6488919 (GenBank accession # NT_039477). Correctly targeted ES cell clones were identified by Southern hybridization of NdeI or NsiI digested DNA with each of probes “a”, “b” and “c” (Fig. 1A). Probe “c” spans nucleotides 6497961 to 6498439 (GenBank accession # NT_039477) and probe “b” is located in neo (Fig. 1A).

4.3. Generation of *HYAL3* deficient mice

Three of seven ES cell clones found to be correctly targeted were aggregated with *CD1* mouse embryos and implanted in pseudo-pregnant *CD1* female mice at the Transgenic and Gene Targeting Facility (Sunnybrook Health Sciences Centre, Toronto, Ontario, Canada) (Nagy et al., 2003). Male chimeras transmitting the targeted *Hyal3* allele were identified for two of the ES cell clones and were used to establish two independent lines of mixed background with *CD1* mice obtained from Central Animal Care Services, University of Manitoba. One of the male chimeras transmitting the *Hyal3* targeted allele in their germ-line was also crossed with 129S1 (Charles River Laboratories, Quebec, Canada) female mice to generate a congenic line. Initially, mice with the targeted *Hyal3* allele were identified by hybridization of NdeI-digested liver DNA with probe “a” (Fig. 1A); later routine genotyping was performed by PCR amplification of tail DNA. For the amplification of the wild-type *Hyal3* allele, the primers were sense 5'-GGTCTCCATCTCTGTGGCAT-3' and antisense 5'-GCAGCCTGCTCAAAGCTAGT-3'. For the amplification of the neo-targeted allele, the primers were sense 5'-TGGCTACCCGTGATATTGCT-3' and antisense 5'-GAGGCTGCCAGGTCGACTGT-3'. Mice with the desired genotypes were obtained from heterozygous and homozygous crosses. All mice were maintained in the Central Animal Care Services at The University of Manitoba following protocols approved by the Animal Care and Use Committee at the University of Manitoba and the guidelines of the Canadian Council on Animal Care. Mice were euthanized at a range of ages, and tissues and serum were collected and assayed as follows.

4.4. Isolation and characterization of total RNA

Total RNA was isolated by the guanidinium thiocyanate-acidic phenol method (Chomczynski and Sacchi, 1987), and the RNA was reverse-transcribed to cDNA using Superscript III (Invitrogen Canada Inc., Burlington, Ontario, Canada) according to the manufacturer's instructions. For real-time PCR, TaqMan Gene Expression Assays (Applied Biosystems Inc. [ABI] for *Hyal1* (Mm00476206_m1), *Hyal2* (Mm0047731_m1), *Hyal3* (Mm00662097_m1), *Hyal4* (Mm01165340_m1), *Hyal5* (Mm01165333_m1), *Spam1* (Mm00486329_m1), *HexB* (Mm00599880_m1), *Fus2* (Mm01947825_s1) and Hypoxanthine-guanine Phospho Ribosyl Transferase 1 (*Hprt1*) (4352339E), or a TaqMan Custom Assay for *Hyalp1* (Primers: sense 5'-GGGAACCCTTCTGTGTTTGAAA-3'; antisense 5'-CCCACTGGATAAACATGGATTGCT-3' and probe 5'-CCTTTGAGCACACTTCC-3') were used. The threshold cycle number (C_T) was determined for the transcripts of the target genes and the *Hprt1* gene in each sample. Experiments for each mouse were performed in duplicate and each sample was analyzed in triplicate; all of the assays were performed using the ABI 7500 Real-time PCR system under the standard cycling conditions suggested by the manufacturer. For conventional reverse transcription (RT)-PCR, primers specific for the wild-type (sense 5'-GACTCTAGATCTGTGGCAAG-3' and antisense 5'-GGTCGTCCAGACAGGAA-3') and the targeted (sense 5'-GGCTACCCGTGATATTGC-3' and antisense 5'-AGGTCGTCCAGACAGGAA-3') alleles were used.

4.5. Analysis of serum HA

Blood was collected from the mice immediately following termination and allowed to clot at room temperature. The serum

was collected by centrifugation and stored at -80 °C. Serum HA concentration was quantified using a HA Test Kit (Corgenix Inc., Broomfield, Colorado, USA) following the manufacturer's instructions.

4.6. Analysis of total tissue GAG content

Tissues to be analyzed for total GAG content were weighed immediately after dissection and frozen by immersion in liquid nitrogen. The tissues were subsequently crushed on dry ice and lyophilized. Total GAGs from the lyophilized tissues were extracted into 5 volumes of 6 M urea, 50 mM Na acetate, 0.1 M Na_2EDTA and 0.1 M aminocaproic acid pH 6.5 at 4 °C for 48 h. The tissue extracts were centrifuged at $7700\times g$ for 25 min at 4 °C and the supernatants were applied to Q-Sepharose resin equilibrated with 50 mM Na acetate, 250 mM NaCl, 10 M formamide pH 6.0. Columns were washed with 10 volumes of the same buffer, and the samples were eluted in the same buffer but containing 5 volumes of 4 M NaCl. GAGs were quantified as uronic acid content (Blumenkrantz and Asboe-Hansen, 1973), and the total GAGs of the tissues were normalized to the tissue wet weight.

4.7. Analysis of total β -hexosaminidase activity

Liver tissues were homogenized in phosphate buffered saline containing 0.1% Triton X-100 and protease inhibitors for tissues as recommended by the manufacturer (Sigma-Aldrich Canada Ltd., Oakville, Ontario, Canada). Cell debris were removed by centrifugation, and the supernatant was used to measure the total β -Hex activity with 4-methylumbelliferyl-2-acetamido-2-deoxy-beta-D-glucopyranoside as a substrate as previously described (Shapira et al., 1989). The protein concentration was determined using a Bio-Rad kit (Bio-Rad laboratories, Hercules, CA, USA) based on the method of Bradford (1976).

4.8. Histological analyses

Tissues were collected and weighed immediately following CO_2 euthanasia. For light microscopy, soft tissues were fixed in 4% paraformaldehyde or formalin, and embedded in paraffin. Sections of 6 μm thickness were stained with either hematoxylin and eosin (12–14 months-of-age) or alcian blue (pH 2.5) and Periodic Acid Schiff reagent (6 months-of-age). Joint tissue from the hind knee was fixed in 0.01 M periodate–0.075 M lysine–0.037 M paraformaldehyde, processed as described previously (Sahebjam et al., 2007), and sections were stained with either toluidine blue or Safranin O.

For electron microscopy, tissues were fixed at 4 °C for 24 h in 2% glutaraldehyde and 2% paraformaldehyde in 0.1 M cacodylate buffer containing 0.5% ruthenium red. Tissues were post-fixed (1 h) in a solution of 1% osmium tetroxide, 0.8% potassium ferricyanide and 0.5% ruthenium red and stained overnight with 2% uranyl acetate. Tissues were dehydrated and embedded in epon. Sections were cut in the histology lab of the Department of Human Anatomy and Cell Science (University of Manitoba) and viewed using a Philips CM 100 transmission electron microscopy.

4.9. Statistical analysis

Comparison of the genotype distribution and sex ratios was performed by Chi-Square analysis with Graphpad QuickCalcs (San Diego, CA, USA). The significance of the real-time RT-PCR data was tested using the unpaired *T*-test (GraphPad QuickCalcs) to compare ΔC_T values. Comparisons of serum HA levels, tissue GAG levels, body weights and organ weights were made with multiway ANOVA or ANOVA statistics using Prism 4 software or NCS software (Kayville, Utah, USA). Significance was defined for all statistical tests at 0.05 ($P < 0.05$).

Acknowledgments

We thank Dr. Andras Nagy and Ms. Marina Gertsenstein for opening their laboratory and providing training to us in ES cell targeting. We also thank Dr. Paul Hazelton and Dr. Jim Thliveris for assistance with electron microscopy and Drs. Martin Reed and Michael Webber for reviewing the X-rays. ES cell targeting was performed at the Canadian Genetic Diseases Network ES Cell Targeting Facility supported by the Canadian Networks for Centres of Excellence.

This research was funded by the Canadian Institutes of Health Research (to BTR, grant # MOP-15463), Shriners of North America (to JM), Natural Sciences and Engineering Research Council (to EC, grant # 262142-04) and National Health and Medical Research Council of Australia (to SB). VA was supported by CIHR strategic training program studentship and University of Manitoba Graduate Fellowship; DM was supported by a studentship from the Manitoba Health Research Council; and SS was supported by the Canadian Arthritis Network of Centers of Excellence.

References

- Adra, C.N., Boer, P.H., Mcburney, M., W.Chaker, N., 1987. Cloning and expression of the mouse pgk-1 gene and the nucleotide sequence of its promoter. *Gene* 60, 65–74.
- Arming, S., Strobl, B., Wechselberger, C., Kreil, G., 1997. In vitro mutagenesis of PH-20 hyaluronidase from human sperm. *Eur. J. Biochem.* 247, 810–814.
- Blumenkrantz, N., Asboe-Hansen, G., 1973. New method for quantitative determination of uronic acids. *Anal. Biochem.* 54, 484–489.
- Bradford, M.M., 1976. A rapid and sensitive method for the quantitation of microgram quantities of protein utilizing the principle of protein-dye binding. *Anal. Biochem.* 72, 248–254.
- Camenisch, T.D., Spicer, A.P., Brehm-Gibson, T., Biesterfeldt, J., Augustine, M.L., Calabro Jr., A., Kubalak, S., Klewer, S.E., McDonald, J.A., 2000. Disruption of hyaluronan synthase-2 abrogates normal cardiac morphogenesis and hyaluronan-mediated transformation of epithelium to mesenchyme. *J. Clin. Invest.* 106, 349–360.
- Chomczynski, P., Sacchi, N., 1987. Single-step method of RNA isolation by acid guanidinium thiocyanate-phenol-chloroform extraction. *Anal. Biochem.* 162, 156–159.
- Chow, G., Knudson, C.B., Knudson, W., 2006. Expression and cellular localization of human hyaluronidase-2 in articular chondrocytes and cultured cell lines. *Osteoarthritis. Cartilage.* 14, 849–858.
- Csoka, A.B., Frost, G.I., Stern, R., 2001. The six hyaluronidase-like genes in the human and mouse genomes. *Matrix Biol.* 20, 499–508.
- Csoka, A.B., Scherer, S.E., Stern, R., 1999. Expression analysis of six paralogous human hyaluronidase genes clustered on chromosomes 3p21 and 7q31. *Genomics* 60, 356–361.
- Culty, M., Nguyen, H.A., Underhill, C.B., 1992. The hyaluronan receptor (CD44) participates in the uptake and degradation of hyaluronan. *J. Cell Biol.* 116, 1055–1062.
- Day, A.J., Prestwich, G.D., 2002. Hyaluronan-binding proteins: tying up the giant. *J. Biol. Chem.* 277, 4585–4588.
- Fraser, J.R.E., Laurent, T.C., Laurent, U.B.G., 1997. Hyaluronan: its nature, distribution, functions and turnover. *J. Int. Med.* 242, 27–33.
- Fraser, J.R.E., Laurent, T.C., 1989. Turnover and metabolism of hyaluronan. *Ciba Found. Symp.* 143, 41–59.
- Harada, H., Takahashi, M., 2007. CD44-dependent intracellular and extracellular catabolism of hyaluronic acid by hyaluronidase-1 and -2. *J. Biol. Chem.* 282, 5597–5607.
- Hemming, R., Martin, D.C., Slominski, E., Nagy, J.I., Halayko, A.J., Pind, S., Triggs-Raine, B., 2008. Mouse Hyal3 encodes a 45- to 56-kDa glycoprotein whose overexpression increases hyaluronidase 1 activity in cultured cells. *Glycobiology* 18, 280–289.
- Jiang, D., Liang, J., Fan, J., Yu, S., Chen, S., Luo, Y., Prestwich, G.D., Mascarenhas, M.M., Garg, H.G., Quinn, D.A., Homer, R.J., Goldstein, D.R., Bucala, R., Lee, P.J., Medzhitov, R., Noble, P.W., 2005. Regulation of lung injury and repair by Toll-like receptors and hyaluronan. *Nat. Med.* 11, 1173–1179.
- Kim, E., Baba, D., Kimura, M., Yamashita, M., Kashiwabara, S., Baba, T., 2005. Identification of a hyaluronidase, Hyal5, involved in penetration of mouse sperm through cumulus mass. *Proc. Natl. Acad. Sci. U. S. A.* 102, 18028–18033.
- Kreil, G., 1995. Hyaluronidases— a group of neglected enzymes. *Protein Sci.* 4, 1666–1669.
- Laurent, U.B.G., Reed, R.K., 1991. Turnover of hyaluronan in the tissues. *Adv. Drug Delivery Rev.* 7, 237–256.
- Lepperdinger, G., Strobl, B., Kreil, G., 1998. HYAL2, a human gene expressed in many cells, encodes a lysosomal hyaluronidase with a novel type of specificity. *J. Biol. Chem.* 273, 22466–22470.
- Martin, D.C., Atmuri, V., Hemming, R.J., Farley, J., Mort, J.S., Byers, S., Hombach-Klonisch, S., Stern, R., Triggs-Raine, B.L., 2008. A mouse model of human mucopolysaccharidosis IX exhibits osteoarthritis. *Hum. Molec. Genet.* 17, 1904–1915.
- Miller, A.D., 2003. Identification of Hyal2 as the cell-surface receptor for jaagsiekte sheep retrovirus and ovine nasal adenocarcinoma virus. *Curr. Top. Microbiol. Immunol.* 275, 179–199.
- Nagy, A., Gertsenstein, M., Vintersten, K., Behringer, R., 2003. Manipulating the mouse embryo: a laboratory manual. Cold Spring Harbor Laboratory Press, Cold Spring Harbor, NY.
- Natowicz, M.R., Short, M.P., Wang, Y., Dickersin, G.R., Gebhardt, M.C., Rosenthal, D.I., Sims, K.B., Rosenberg, A.E., 1996. Clinical and biochemical manifestations of hyaluronidase deficiency. *New Engl. J. Med.* 335, 1029–1033.
- Rai, S.K., Duh, F.M., Vigdorovich, V., Danilkovitch-Miagkova, A., Lerman, M.I., Miller, A.D., 2001. Candidate tumor suppressor HYAL2 is a glycosylphosphatidylinositol (GPI)-anchored cell-surface receptor for jaagsiekte sheep retrovirus, the envelope protein of which mediates oncogenic transformation. *Proc. Natl. Acad. Sci. U. S. A.* 98, 4443–4448.
- Roden, L., Campbell, P., Fraser, J.R.E., Laurent, T.C., Pertoft, H., Thompson, J.N., 1989. Enzymic pathways of hyaluronan catabolism. *Ciba Found. Symp.* 143, 60–86.
- Sahebjam, S., Khokha, R., Mort, J.S., 2007. Increased collagen and aggrecan degradation with age in the joints of Timp3(−/−) mice. *Arthritis Rheum.* 56, 905–909.
- Shapira, E., Blitzer, M.G., Miller, J.B., Africk, D.K., 1989. Biochemical genetics: a laboratory manual. Oxford University Press, Oxford, NY.
- Shuttleworth, T.L., Wilson, M.D., Wicklow, B.A., Wilkins, J.A., Triggs-Raine, B.L., 2002. Characterization of the murine hyaluronidase gene region reveals complex organization and cotranscription of Hyal1 with downstream genes, Fus2 and Hyal3. *J. Biol. Chem.* 277, 23008–23018.
- Stern, R., Jedrzejewski, M.J., 2006. Hyaluronidases: their genomics, structures, and mechanisms of action. *Chem. Rev.* 106, 818–839.
- Triggs-Raine, B., Salo, T., Zhang, H., Wicklow, B.A., Natowicz, M., 1999. Mutations in HYAL1, a member of a tandemly distributed multigene family encoding disparate hyaluronidase activities, cause a newly described lysosomal disorder, mucopolysaccharidosis IX. *Proc. Natl. Acad. Sci. U.S.A.* 96, 6296–6300.
- Zegerman, P., Bannister, A.J., Kouzarides, T., 2000. The putative tumour suppressor Fus-2 is an N-acetyltransferase. *Oncogene* 19, 161–163.